

Influence of Modeling Assumptions on the Inferred Dynamical State of Resonant Systems: A Case Study of the HD 45364 System

IAN CHOW ^{1,2,3} AND SAM HADDEN ⁴

¹*David A. Dunlap Department of Astronomy & Astrophysics, University of Toronto, 50 St George Str, Toronto, ON M5S 3H4, Canada*

²*Department of Physics and Astronomy, University of Western Ontario, 1151 Richmond Str, London, ON N6A 3K7, Canada*

³*Institute for Earth and Space Exploration, University of Western Ontario, Perth Drive, London, ON N6A 5B7, Canada*

⁴*Canadian Institute for Theoretical Astrophysics, 60 St George Str, Toronto, ON M5S 3H8, Canada*

(Published 2025 February 19)

ABSTRACT

Planetary systems exhibiting mean-motion resonances (MMRs) offer unique opportunities to study the imprint of disk-induced migration on the orbital architectures of planetary systems. The HD 45364 system, discovered via the radial velocity (RV) method to host two giant planets in a 3:2 MMR, has been the subject of several studies attempting to reconstruct the system’s orbital migration history based on its present-day resonant configuration. Recently, Li et al. (2022) called into question the system’s residence in the 3:2 MMR based on a revised orbital solution derived from an expanded set of RV observations that extend the time baseline of the original discovery data by over a decade. However, we show that inferences about the planets’ dynamical state with respect to the 3:2 MMR are sensitive to the particular prior assumptions adopted in the orbital modeling. Using N -body dynamical models, we show that orbital solutions constrained to reside deep in the 3:2 MMR fit the RV data with a similar quality to unconstrained orbital solutions. We conclude that the RV observations of HD 45364 are consistent with orbital configurations produced by smooth migration and resonance capture. We further show that past convergent orbital migration can reproduce the system’s present-day orbital configuration provided that the ratio of migration to eccentricity damping timescales, K , was in the range $11 \lesssim K \lesssim 144$. We also find that dynamical interactions in the system can break the usual mass-inclination degeneracy inherent to Keplerian models of RV observations and constrain the planets’ absolute masses to within a factor of ~ 1.5 .

Keywords: Exoplanets (498) – Orbital resonances (1181) – Exoplanet dynamics (490) – Celestial mechanics (211) – Radial velocity (1332)

1. INTRODUCTION

Numerous pairs of giant planets in mean-motion resonances (MMRs) have been discovered via the radial velocity (RV) method (e.g. Mayor et al. 2004; Lee et al. 2006; Tinney et al. 2006; Correia et al. 2009; Niedzielski et al. 2009; Johnson et al. 2010, 2011; Wright et al. 2011; Robertson et al. 2012; Wittenmyer et al. 2013, 2016; Giguere et al. 2015; Luque et al. 2019; Trifonov et al. 2019). The resonant orbital configurations of these systems are generally interpreted as products of past convergent orbital migration induced by planet interactions with the protoplanetary disk (Goldreich & Tremaine 1980), as such migration generically causes planets to be captured into any low-order MMRs they encounter. Thus, systems hosting resonant planets present attrac-

tive choices for studying orbital migration and its role in planetary formation.

One such system is HD 45364, which consists of a K0V star with mass of $0.82 M_{\odot}$ and two approximately Jupiter-mass planets with orbits near a 3:2 commensurability, discovered by Correia et al. (2009) using the High Accuracy Radial Velocity Planet Searcher (HARPS; Mayor et al. 2003). The original best-fit RV solution of Correia et al. (2009) indicated that the two planets were on slightly eccentric orbits and experienced large librations within the 3:2 MMR, with $\sim 70^{\circ}$ excursions of the resonant angles away from their equilibrium values. Subsequent work by Rein et al. (2010) used hydrodynamical simulations of planet-disk interactions to find potential migration histories that could produce or-

bital configurations that were consistent with the observed RV data. They found orbital solutions arising from their migration simulations that differed significantly from the best-fit solution reported by [Correia et al. \(2009\)](#) but which reproduced the observed data with approximately equal statistical significance. Similar conclusions were reached by [Correa-Otto et al. \(2013\)](#) using N -body simulations with parameterized migration and eccentricity damping forces. Finally, [Hadden & Payne \(2020\)](#) showed, using a Bayesian model comparison framework, that the available RV data for HD 45364 were fully consistent with the planet pair residing in a zero-libration amplitude resonant configuration that would naturally arise under the effects of smooth migration and eccentricity damping forces.

New RV measurements of HD 45364 by the HARPS team, available through the HARPS-RVBank archive ([Trifonov et al. 2020](#)), as well as observations from the High Resolution Echelle Spectrometer (HIRES; [Vogt et al. 1994](#)) instrument, obtained by [Li et al. \(2022\)](#), have significantly extended the observational baseline of the original data set analyzed in the studies described above. Based on orbital fitting of this extended data set, [Li et al. \(2022\)](#) conclude that the HD 45364 planets are slightly outside of the 3:2 MMR, contrary to the conclusions of previous studies and the theoretical expectations for any planet pair migrated into a compact configuration via planet-disk interactions.

However, as emphasized by both [Hadden & Payne \(2020\)](#) and [Jensen & Millholland \(2022\)](#), inferences about the dynamical state of (near-)resonant planet pairs can be particularly sensitive to modeling assumptions. Indeed, [Jensen & Millholland \(2022\)](#) show that measurement noise in RV observations tends to produce a bias towards larger libration amplitudes of planets in MMR. This is essentially because orbital configurations with large libration amplitudes occupy significantly more prior volume than low-libration amplitude configurations.

In this paper, we re-analyze the recently-extended data set of RV measurements for the HD 45634 system in order to explore how the system’s inferred dynamical state with respect to the 3:2 MMR is influenced by modeling assumptions. Following [Jensen & Millholland \(2022\)](#), we explore how the system’s dynamical state is influenced by the assumed Bayesian priors on planets’ orbital parameters. We also show that un-modeled measurement noise can masquerade as a significant libration amplitude in the system.

This paper is structured as follows: In Section 2, we present our orbital fitting procedures, fit an RV curve to observations with an N -body dynamical model and es-

timate posterior distributions for the model parameters. We then investigate how the system’s inferred dynamical state is affected by assumptions about measurement noise and by different priors on the model parameters. In Section 3 we give a brief review of the dynamics of resonance capture and analyse possible scenarios for the migration of HD 45364’s planets assuming an MMR configuration. We summarize our conclusions in Section 4.

2. RADIAL VELOCITY FITTING

The original RV observations of HD 45364 used by [Correia et al. \(2009\)](#) were taken by the HARPS telescope over a period of approximately 1600 days from December 2003 to April 2008. Further observations of the system by HARPS have since extended its observational baseline to September 2017, spanning over 5000 days in total. [Trifonov et al. \(2020\)](#) improved the HARPS RV precision by recomputing the RVs from observed spectra using the Spectrum Radial Velocity Analyser pipeline of [Zechmeister et al. \(2018\)](#) and correcting a number of systematic errors. The new HARPS data were later published as part of the HARPS-RVBank archive¹([Trifonov et al. 2020](#)), totalling 122 RV observations. In addition, an upgrade to HARPS’s optical fibres in May 2015 ([Lo Curto et al. 2015](#)) changed the instrumental profile and thus the RV offset between the pre- and post-upgrade RV observations ([Trifonov et al. 2020](#)). As such, we treat the pre- and post-upgrade RV data as taken from two separate instruments in this work. Finally, we also use 7 RV observations taken by HIRES from December 2009 to September 2021, provided in Table 1 of [Li et al. \(2022\)](#).

Here we report our fits to the full set of RV data available for HD 45634, consisting of 129 data points spanning a total observational baseline of ~ 6500 days.² We begin in Section 2.1 by describing our N -body dynamical model, which we fit under relatively uninformative priors on the planets’ orbital parameters. In Section 2.2, we explore how the inferred dynamical state of the system with respect to the 3:2 MMR is influenced by the model priors and assumptions about the level of measurement noise.

2.1. N -body dynamical model

We fit the RV observations of HD 45364 using an N -body model that accounts for Newtonian gravitational

¹ github.com/3fon3fonov/HARPS_RVBank

² We note that [Li et al. \(2022\)](#) use only 121 total data points (114 from HARPS and 7 from HIRES) in their analysis, as in two separate cases, they combine five HARPS observations taken over a short time span into a single observation.

interactions among the star and two planets in order to compute the star’s RV. Integrations for this dynamical model and all other simulations presented in this paper are conducted with the `REBOUND` (Rein & Liu 2012) code for numerical N -body integration, using the `IAS15` integrator (Rein & Spiegel 2015) for the integration and Jacobi elements for the coordinate frame. We fit our model to three sets of RV observations: the pre- and post-upgrade HARPS observations (which we denote HARPS1 and HARPS2 respectively), and the HIRES observations.

The planets’ orbits are parameterized in terms of their orbital periods, P_i , eccentricities, e_i , times of conjunction, T_i , and arguments of pericenter, ω_i , all specified at a reference epoch of $t_0 = 54422.79 + 2.4 \times 10^6$ BJD. This value is chosen as the median time of the RV observations for the system. We parameterize the planets’ masses, m_i , in our model as functions of the planets’ orbital parameters and RV semi-amplitudes, K_i , according to

$$m_i = \left(\frac{2\pi G}{P_i} \right)^{-1/3} M_*^{2/3} \frac{K_i}{\sin I} \sqrt{1 - e_i^2} \quad (1)$$

where M_* is the host star mass (which we fix to be $M_* = 0.82 M_\odot$), and G is Newton’s universal gravitational constant. We assume the planets’ orbits to be coplanar but allow their orbital planes to be inclined with respect to the sky plane by an angle, I , and include $\sin(I)$ as a free parameter in our N -body model. Our model also includes RV offsets, γ_j , for the three sets of observations HARPS1, HARPS2, and HIRES. Finally, our model includes three instrumental jitter parameters $\sigma_{\text{jit},j}$, one for each set of observations. Writing $\boldsymbol{\theta}_{\text{orb}} = \{\sin I\} \cup \{K_i, P_i, e_i, T_i, \omega_i\}_{i=1}^2$ to denote the subset model parameters governing the orbital data, the log-likelihood of a set of model parameters can be written as

$$\begin{aligned} \ln \mathcal{L}(\boldsymbol{\theta}, \boldsymbol{\gamma}_j, \boldsymbol{\sigma}_{\text{jit},j}) = & - \sum_{j=1}^3 \sum_{i=1}^{N_j} \frac{(v_{j,i} - \gamma_j - \bar{v}_{j,i}(\boldsymbol{\theta}_{\text{orb}}))^2}{2(\sigma_{j,i}^2 + \sigma_{\text{jit},j}^2)} \\ & - \sum_{i=1}^{N_j} \ln \sqrt{2\pi(\sigma_{j,i}^2 + \sigma_{\text{jit},j}^2)} \quad (2) \end{aligned}$$

where the index j runs over the three sets of RV data from HARPS1, HARPS2, and HIRES, $v_{j,i}$ denotes i th observed RV from the j th set of observations, $\sigma_{j,i}$ denotes this velocity’s reported measurement uncertainty, and $\bar{v}_{j,i}(\boldsymbol{\theta}_{\text{orb}})$ denotes the star’s RV predicted by our N -body dynamical model at the time of observation.

We use Markov Chain Monte Carlo (MCMC) sampling to estimate the posterior distribution of our model

parameters. We adopt priors that are uniform on the interval $[0, \infty)$ for planets’ orbital periods, P_i , semi-amplitudes, K_i , and times of conjunction, T_i . Our prior on the sine of the planets’ orbital inclination, $\sin I$, is uniform between 0 and 1. We adopt the standard procedure of parameterizing planets’ orbital eccentricities, e_i , and arguments of pericenter, ω_i , by the variables $\sqrt{e_i} \cos \omega_i$ and $\sqrt{e_i} \sin \omega_i$ when sampling, while imposing a prior that planets’ eccentricities be less than 1. Finally, our priors on the value of the instrumental jitters, $\sigma_{\text{jit},j}$, are uniform between 0 and 10 m s^{-1} . The MCMC sampling is carried out using the `emcee` (Goodman & Weare 2010; Foreman-Mackey et al. 2013) software package. We initialize 50 chains in a multivariate Gaussian distribution centered on the best-fit parameters obtained by minimizing the log-likelihood. The chains are then evolved for 50,000 steps, generating a total of 2.5 million posterior samples. We compute the autocorrelation lengths of our MCMC chains for each model parameter and estimate that our simulations produce $\gtrsim 3000$ independent posterior samples by dividing the total number of samples by the longest computed autocorrelation length.

The resulting RV fit is shown in Figure 1. The top panel shows the 1σ , 2σ and 3σ uncertainties of our fit RV curve together with the observed data. We obtain best-fit instrumental jitter values of 1.41, 0.694 and 3.00 m s^{-1} for the HARPS1, HARPS2 and HIRES telescopes, respectively. The maximum log-likelihood solution and the 5%, 50% and 95% quantiles of the 1D posterior distributions obtained from MCMC sampling are reported in Table 2.1.

The large masses and close orbits of the two planets in HD 45364 give rise to mutual gravitational interactions between the planet pair that are strong enough for our dynamical model to break the usual $m \sin I$ degeneracy inherent to purely Keplerian models. We therefore let inclination vary as a free parameter in our model, allowing us to place constraints on the planet masses and inclinations. Using our dynamical model, we constrain the absolute masses of HD 45364 b and c to within a factor of ~ 1.5 of the median values. Figure 2 shows marginalized joint posterior distributions of planet masses versus $\sin I$. The posterior density falls off sharply for $\sin I \lesssim 0.6$. Furthermore, we find through N -body ex-

Table 1. Maximum Log-Likelihood Fit and MCMC Posterior Quantiles for Fitted Parameters

Parameter	Maximum Log-Likelihood	MCMC Posterior Quantiles		
$\ln \mathcal{L}$	-246.78			
		5%	50%	95%
$m_b [M_J]$	0.191	0.191	0.222	0.320
P_b [days]	227.88	227.20	227.93	228.69
e_b	0.0505	0.0328	0.0613	0.0917
T_b [BJD - 2.4×10^6 days]	52799.70	52793.08	52801.02	52808.58
ω_b [rad]	-2.95	-3.03	-2.51	2.94
$m_c [M_J]$	0.550	0.557	0.641	0.932
P_c [days]	344.06	343.53	344.01	344.49
e_c	0.00991	0.00132	0.0136	0.0353
T_c [BJD - 2.4×10^6 days]	52985.87	52982.85	52986.16	52989.33
ω_c [rad]	1.34	-1.99	1.03	2.51
$\sin(I)$	1.00	0.594	0.860	0.988
$\sigma_{\text{jit,HARPS1}}$ [m/s]	1.41	1.19	1.50	1.76
$\sigma_{\text{jit,HARPS2}}$ [m/s]	0.694	0.17	0.96	1.66
$\sigma_{\text{jit,HIRES}}$ [m/s]	3.00	1.89	4.00	7.57

Note. The orbital periods P_i , times of conjunction T_i , eccentricities e_i and arguments of pericenter ω_i are osculating parameters valid for the reference epoch $t_0 = 2454422.79$ BJD.

periments that the dynamical stability of the system demands that $\sin I \gtrsim 0.1$.³

2.2. The influence of model priors and measurement noise on resonant dynamics

The solid lines in Figure 3 show the cumulative distribution for the maximum deviation of the planets’ resonant angles from equilibrium, measured from short N -body integrations spanning 500 orbits of the inner planet for a random selection of 50,000 samples from our full MCMC posterior. For each posterior sample, the resonant angles $\theta_b = 3\lambda_c - 2\lambda_b - \varpi_b$ and $\theta_c = 3\lambda_c - 2\lambda_b - \varpi_c$ were recorded at 5000 uniformly spaced times in the integration and the maximum deviations from their respective equilibrium values of 0 and π were computed. Figure 3 clearly indicates that most of the posterior samples have large libration amplitudes, with roughly half of the posterior samples showing libration amplitudes greater than 90° in both resonant angles and a majority of posterior samples ($\gtrsim 60\%$) showing circulation in angle θ_c . These results nominally support the conclusion

of Li et al. (2022) that the HD 45364 planets are not fully locked in the 3:2 MMR.⁴

However, Jensen & Millholland (2022) demonstrate that measurement noise can cause a systematic bias to resonant libration amplitudes inferred from RVs. This bias is essentially caused by the fact that higher libration amplitude dynamical configurations occupy a much larger phase-space volume. Consequently, under model priors that are relatively uniform over phase space, noisier data will lead to broader posterior distributions that, in turn, become increasingly skewed towards large libration amplitudes or circulating resonant angles. In this section, we explore the sensitivity of the inferred resonant libration amplitudes of the HD 45364 planets to assumptions about measurement noise and model priors.

To explore the influence of model priors on the inferred resonant behaviour of the HD 45364 planets, we follow Jensen & Millholland (2022) and test a series of priors that penalize dynamical configurations according to their libration amplitudes measured in short N -body integrations. Specifically, we construct a series of priors weighted towards resonant configurations in which

³ The N -body dynamical model MCMC simulations by Li et al. (2022) instead assume the planet pairs’ inclinations are fixed at 90° . They do, however, perform maximum-likelihood fits to the RV data for a series of fixed system inclinations. Comparing the maximum likelihoods as a function of system inclination, they find similar results, concluding that $\sin I \gtrsim 0.6$.

⁴ Strictly speaking, the circulation of θ_c does not preclude the system’s residence in the 3:2 MMR (see, e.g. Petit et al. 2020). However, resonance capture via smooth migration is expected to produce resonant configurations with small libration amplitudes, nominally at odds with the posterior distribution of libration amplitudes.

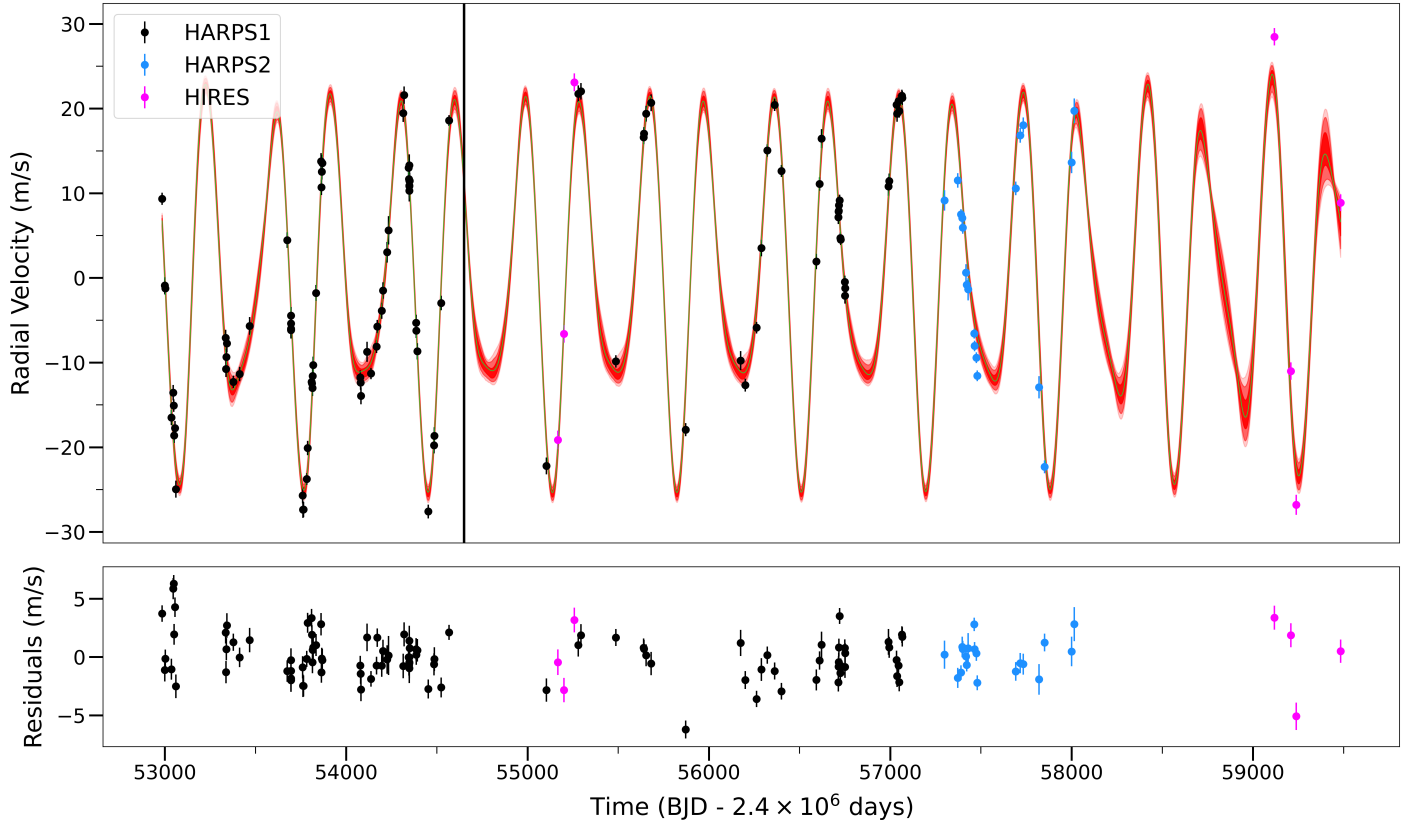


Figure 1. Summary of RV fitting results and uncertainties from the MCMC posterior distributions for HD 45364, using data from the pre- and post-upgrade HARPS (HARPS1 and HARPS2, respectively) and the HIRES instruments. The top panel shows our fit RV signal plotted over the observed RVs, with 1σ , 2σ and 3σ uncertainties illustrated by the red shaded regions. The maximum log-likelihood solution is plotted as the green line. The HARPS data points to the right of the black line are new data obtained from the HARPS-RVBank archive (Trifonov et al. 2020) since the original analysis of Correia et al. (2009). Time is given in units of Barycentric Julian Date (BJD) - 2.4×10^6 days. The normalized residuals of the best-fit solution are plotted in the bottom panel.

we multiply the standard prior probability of a set of model parameters described above in Section 2.1 by a term $\propto \exp\left[-\frac{1}{2S^2}A_{\text{lib}}^2\right]$, where A_{lib} is the libration amplitude measured as the root-mean-square difference between the resonant angles $\theta_b = 3\lambda_c - 2\lambda_b - \varpi_b$ and $\theta_c = 3\lambda_c - 2\lambda_b - \varpi_c$ and their respective equilibrium values of 0 and π . For a given set of model parameters, we record the values of resonant angles θ_b and θ_c at 1000 uniformly spaced times from N -body integrations spanning 500 orbits of the inner planet and compute A_{lib} according to

$$A_{\text{lib}}^2 = \frac{1}{1000} \sum_{j=1}^{1000} \left(\theta_{b_j}^2 + (\theta_{c_j} - \pi)^2 \right). \quad (3)$$

In Figure 4 we explore the relationship between the assumed level of measurement noise and the inferred libration amplitudes. In order to do so, we first construct a modified likelihood function, \mathcal{L}' , that depends on the orbital model parameters, $\boldsymbol{\theta}_{\text{orb}}$, RV offsets, γ_j , a jitter

scale factor, f , and a libration amplitude scale factor, S , according to

$$\ln \mathcal{L}'(\boldsymbol{\theta}_{\text{orb}}, \gamma_j; f, S) = \ln \mathcal{L}(\boldsymbol{\theta}_{\text{orb}}, \gamma_j, f \hat{\sigma}_{\text{jit},j}) - \frac{A_{\text{lib}}^2(\boldsymbol{\theta}_{\text{orb}})}{2S^2} \quad (4)$$

where \mathcal{L} is the likelihood function of our uninformative prior RV model given in Equation (2) and $\hat{\sigma}_{\text{jit},j}$ are the best-fit jitter values determined via a maximum-likelihood fit to the RV data using the uninformative prior RV model. In Figure 4, we numerically maximize the modified log-likelihood, $\ln \mathcal{L}'$, on a grid of fixed values for the parameters f and S . We then plot contour levels of $\ln \mathcal{L}$, i.e., the *unmodified, uninformative* RV model log-likelihood, evaluated at the numerically determined parameters that maximize the *modified* likelihood, \mathcal{L}' . The $n\sigma$ confidence regions are estimated as $\Delta \ln \mathcal{L} = -\frac{1}{2}n^2$, where $\Delta \ln \mathcal{L}$ is the difference between the log-likelihood function and its global maximum value. If the data strongly favored dynamical con-

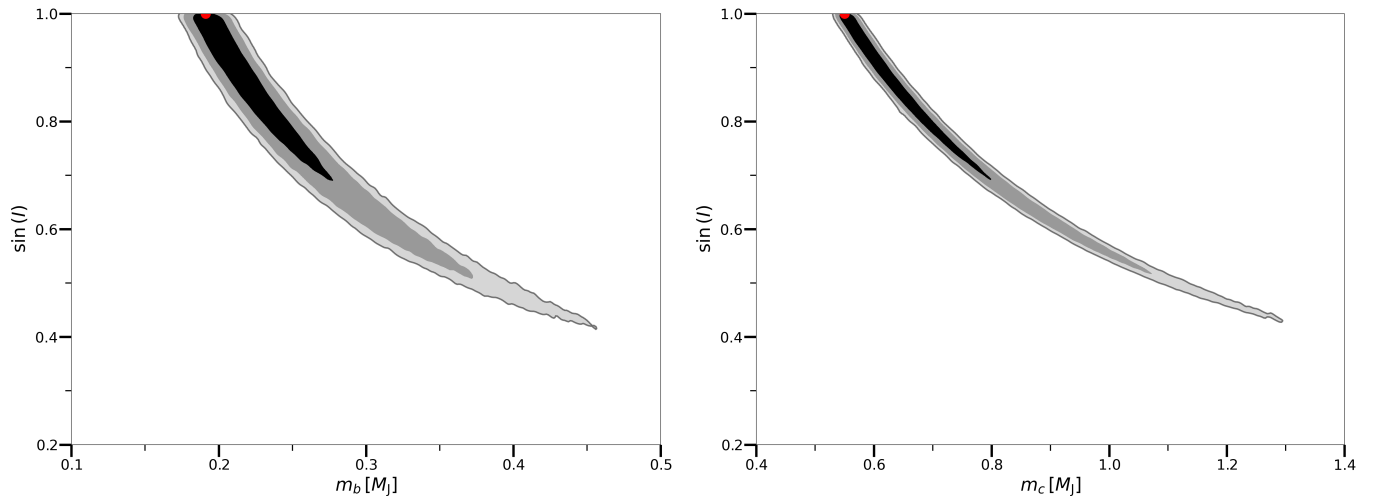


Figure 2. The marginal 2D MCMC posterior distributions of $\sin(I)$ against planet masses m_b (left) and m_c (right), with the planets assumed to be in coplanar orbits. The contours show the 1σ , 2σ and 3σ bounds of the posterior distribution. The points corresponding to the best-fit solution obtained by maximizing the log-likelihood $\ln \mathcal{L}$ as given in Table 1 are marked in red.

figurations in which the resonant angles circulated or possessed large libration amplitudes, we would expect to find that the values of $\ln \mathcal{L}$ decrease significantly for sufficiently small values of S . However, this is not what we see in Figure 4. Instead, contours of constant likelihood are nearly independent of the assumed value of S except at the lowest values of the jitter scaling factor, f . Thus, we conclude that the prevalence of dynamical configurations with circulating and large libration amplitude resonant angles found among the posterior samples of our uninformative prior RV model is the result of these dynamical configurations occupying larger prior volume, rather than the data disfavoring low libration amplitude configurations. Furthermore, the fact that low libration amplitude solutions become disfavored relative to higher amplitude solutions for small values of f indicates that underestimated measurement noise can lead one to improperly infer large libration amplitudes.

To further explore the influence of prior assumptions on the inferred dynamical state of the HD 45364 system, we run a second MCMC sampling simulation implementing the modified “resonance-weighted” prior, $\propto \exp[-\frac{1}{2S^2}A_{\text{lib}}^2]$, with the value of S set to $S = 0.1$. The MCMC sampling was carried out with the same procedure described in Section 2.1, but using the modified log-likelihood function $\ln \mathcal{L}'$ with $S = 0.1$ instead of the unmodified log-likelihood function $\ln \mathcal{L}$. As in Section 2.1, 50 chains were initialized in a multivariate Gaussian distribution centered on the best-fit parameters and each evolved for 50,000 steps, generating a total of 2.5 million posterior samples. The chains successfully converged, with an estimated effective sample size of $\gtrsim 4000$. We compute the resonant angles’ maximum deviation from equilibrium for 50,000 random samples

from the resonance-weighted prior model’s MCMC posterior using the same method as for the uninformative prior model, and plot their cumulative distributions as the dashed lines in Figure 3. We find that virtually all posterior samples generated with our modified priors have resonant angles that librate with small amplitude ($< 90^\circ$), demonstrating that our choice of model priors affects the inferred libration amplitudes.

3. MIGRATION HISTORY

Here we explore possible planetary migration scenarios resulting in the capture of HD 45364’s planets into their current orbital configuration, assuming the system is in MMR. We first provide a brief overview of the dynamics of resonance capture and describe our parameterized model of planetary migration in Section 3.1. Section 3.2 shows our results for possible migration histories of HD 45364 under the modified prior used in Section 2.2.

3.1. Resonance Capture

Tidal interactions between planets and a proto-planetary disk can cause their orbits to migrate and their eccentricities to damp (Lin & Papaloizou 1979; Goldreich & Tremaine 1980). Pairs of planets undergoing convergent migration will tend to be captured into any first-order MMRs they encounter, provided their migration rates are sufficiently slow (e.g., Murray & Dermott 2000). After encountering a resonance, the planet pair will migrate together while maintaining a fixed period ratio and experience eccentricity growth until the resonant forcing of their eccentricities is counterbalanced by the damping effects of the disk (Snellgrove et al. 2001; Lee & Peale 2002). For sufficiently smooth and slow mi-

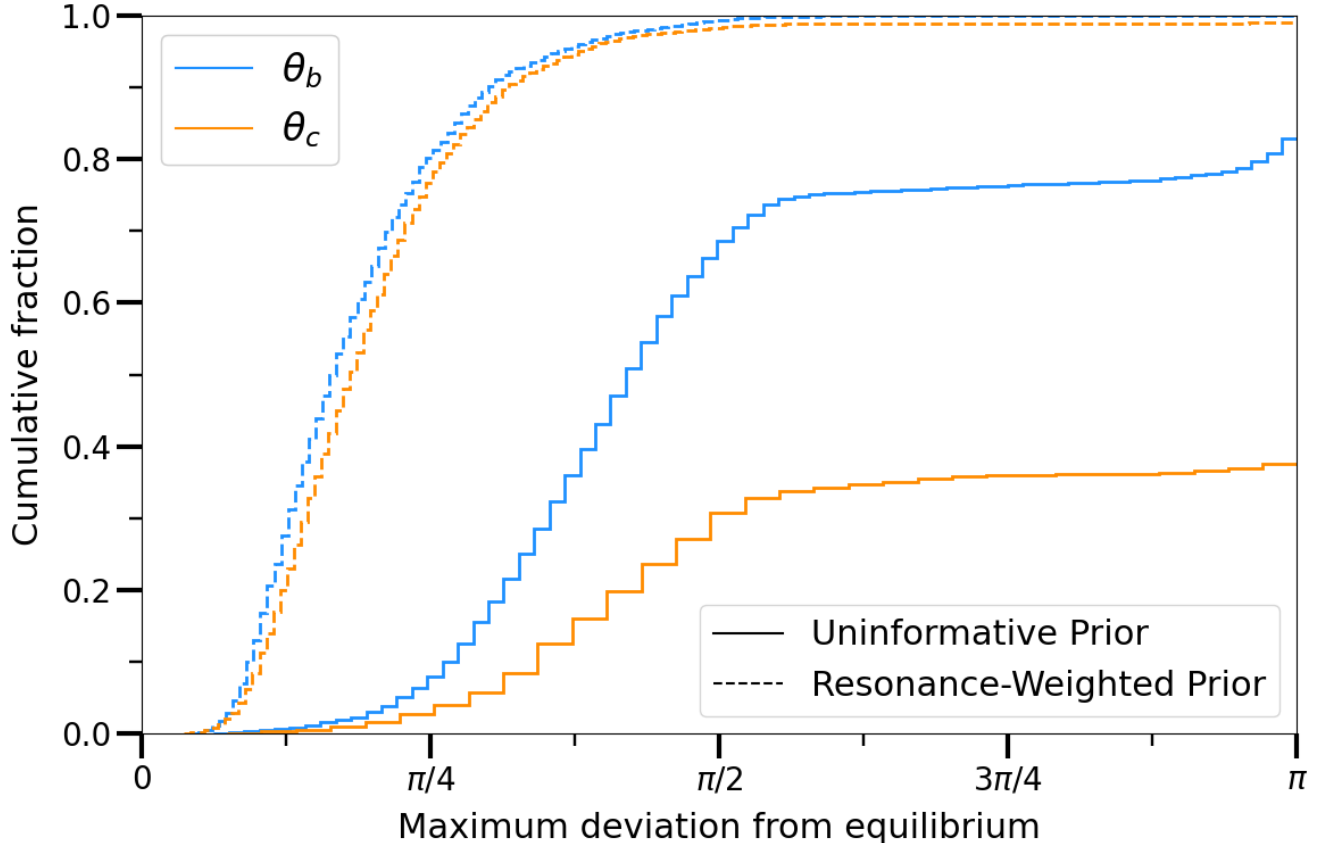


Figure 3. The cumulative distribution of the maximum deviation from equilibrium for the resonant angles θ_b (blue) and θ_c (orange), measured over short N -body integrations, of 50,000 samples drawn randomly from the MCMC posteriors for the N -body dynamical model fit under uninformative priors described in Section 2.1 (solid lines) and the model described in Section 2.2 fit under a resonance-weighted prior (i.e. weighted toward small libration amplitudes), with $S = 0.1$ (dashed lines). A large fraction of orbital configurations in the uninformative prior model’s MCMC posteriors circulate or have large libration amplitudes ($> 90^\circ$). In contrast, virtually all resonant angles in the resonance-weighted prior model’s MCMC posteriors have small libration amplitudes ($< 90^\circ$), showing that the chosen model priors strongly affect the inferred libration amplitudes of the system.

gration forces, the pair of planets will eventually settle into an equilibrium configuration in which their resonant angles and eccentricities remain fixed. As discussed in Hadden & Payne (2020), for a given pair of planet masses and a specific $j:j-1$ resonance, these equilibrium configurations constitute a one-parameter family of orbital configurations that can be parameterized by the quantity

$$\mathcal{D} = \beta_1 \sqrt{\alpha} \frac{e_1^2}{2} + \beta_2 \frac{e_2^2}{2} - \frac{\beta_1 \beta_2 \sqrt{\alpha}}{3(j\beta_1 \sqrt{\alpha} + (j-1)\beta_2)} \Delta, \quad (5)$$

where e_i are the planets’ eccentricities, $\beta_i = m_i/(m_1 + m_2)$, $\alpha \approx \left(\frac{j-1}{j}\right)^{2/3}$ is the pair’s semimajor axis ratio, and $\Delta = \frac{j-1}{j} \frac{P_2}{P_1} - 1$ measures the pair’s fractional deviation from exact period ratio commensurability.

If the the migration and eccentricity damping effects of planet-disk interactions are approximated as exponential decays so that

$$\left. \frac{d}{dt} \ln(a_i) \right|_{\text{dis}} = -\tau_{a,i}^{-1} \quad (6)$$

$$\left. \frac{d}{dt} \ln(e_i) \right|_{\text{dis}} = -\tau_{e,i}^{-1}, \quad (7)$$

then the ultimate equilibrium configuration into which a planet pair settles will be the one for which

$$\left. \frac{d}{dt} \mathcal{D} \right|_{\text{dis}} = 0 \approx -\frac{\beta_1 \sqrt{\alpha} e_1^2}{\tau_{e,1}} - \frac{\beta_2 e_2^2}{\tau_{e,2}} - \frac{\beta_1 \beta_2 \sqrt{\alpha}}{3(j\beta_1 \sqrt{\alpha} + (j-1)\beta_2)} \frac{3}{2\tau_\alpha}, \quad (8)$$

where $\tau_\alpha := (\tau_{a,2}^{-1} - \tau_{a,1}^{-1})^{-1}$. Therefore, the resonant equilibrium reached by a pair of migrating planets de-

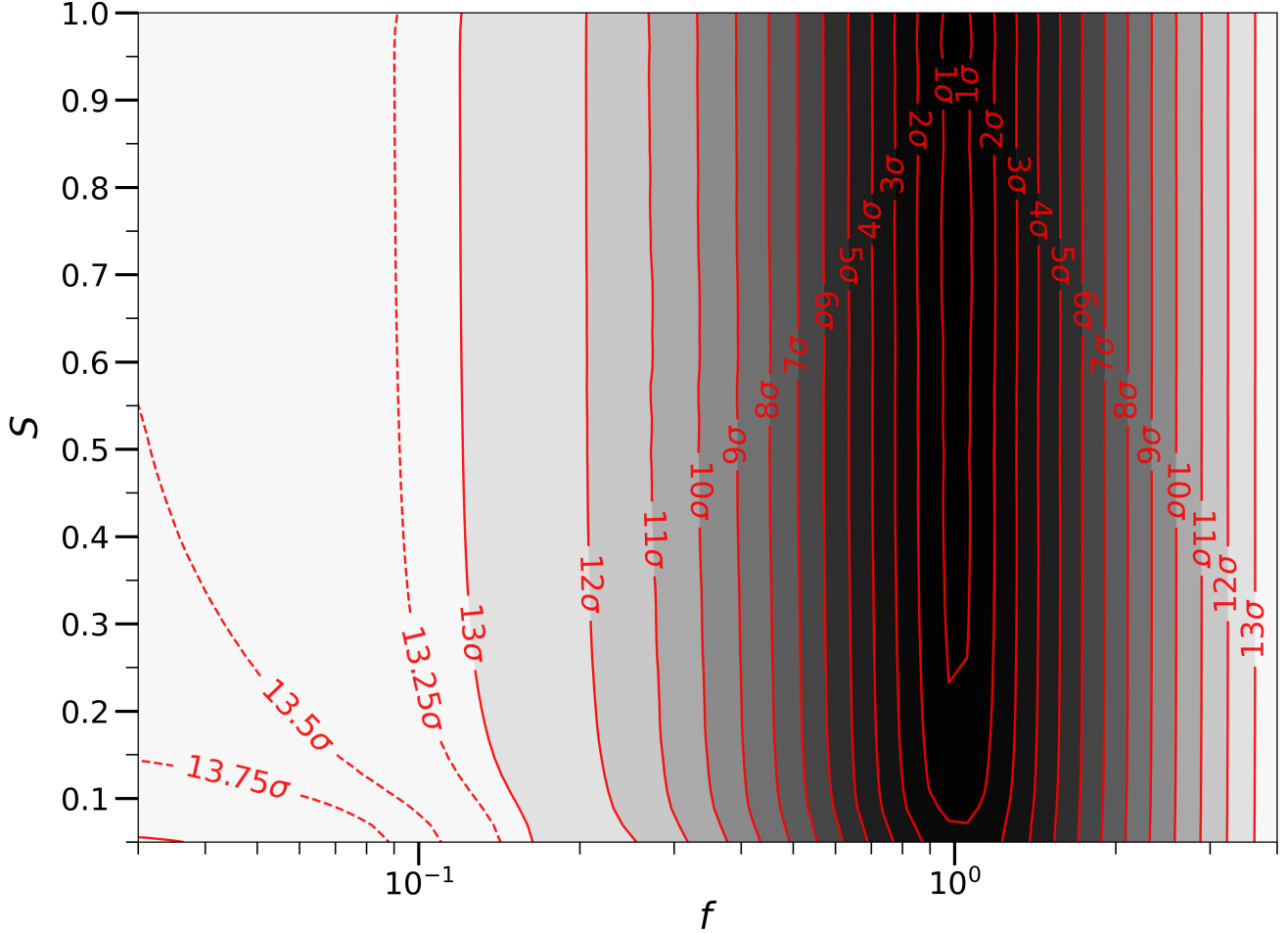


Figure 4. A contour plot of the log-likelihood $\ln \mathcal{L}$ of best-fit orbital solutions found by maximizing the *modified* log-likelihood, $\ln \mathcal{L}'$, given by Equation (4), for different levels of the jitter scale factor, f , and libration amplitude penalty, S . Contours labeled $n\sigma$ mark the log-likelihood levels $\Delta \ln \mathcal{L} = -\frac{1}{2}n^2$, where $\Delta \ln \mathcal{L}$ is the log-likelihood function minus its global maximum value. Dashed contours have been linearly spaced at intervals of 0.25σ between 13σ and 14σ to show that low libration amplitude configurations may be erroneously ruled out compared to high libration amplitude configurations when instrumental jitter is not properly accounted for.

depends on the relative strengths of migration and eccentricity damping forces, frequently parameterized as $K_1 = \tau_\alpha/\tau_{e,1}$ and $K_2 = \tau_\alpha/\tau_{e,2}$.

Figure 5 shows the eccentricities of a pair of planets in the family of 3:2 resonant equilibria. The planets’ masses are taken to be the median masses of HD 45364 b and c, as inferred from our MCMC simulations in Section 2.2. The equilibrium configurations are found by running a series of N -body simulations with eccentricity and semimajor axis damping forces included. We use the `reboundx` code’s (Tamayo et al. 2020) `modify_orbits_direct` effect to impose dissipative forces of the form of Equation (6) and (7). We set the planets’ eccentricity damping timescales to $\tau_{e,b} = \tau_{e,c} =: 2\tau_e = 10^4 P_b$. The semimajor axis damping

timescales, $\tau_{a,i}$, are chosen so that $K = \tau_\alpha/\tau_e$ ranges from 1 to 10^3 and $\tau_{a,b}/\tau_{a,c} = -\frac{m_b}{m_c} \left(\frac{3}{2}\right)^{2/3}$.⁵ The planets are initially placed in circular, coplanar orbits with a period ratio of $P_c/P_b = 1.1 \times \frac{3}{2}$, just outside the 3:2 MMR. The simulations are then integrated until the planets reach their equilibrium eccentricities. Plotting the equilibrium eccentricities of each simulation in Figure 5 produces an eccentricity “track,” along which each simulation evolves after capturing into resonance until

⁵ The latter condition is imposed for numerical convenience, as it ensures that the system remains at approximately the same mean stellocentric distance over the course of the simulations, obviating the need to adjust the simulation time step.

it reaches its unique stopping point at which Equation (8) is satisfied (see Hadden & Payne 2020).

3.2. Results

We determine possible migration scenarios for HD 45364 based on the posterior distribution of orbital configurations from the resonance-weighted prior model described in Section 2.2. Eccentricity posterior samples from our MCMC simulations with this model are plotted in Figure 5. Comparing the inferred distribution of the planets’ eccentricities to the range of equilibrium eccentricities generated by N -body simulations, we can estimate the relative strengths of eccentricity damping to orbital migration that led to the planets’ capture into the 3:2 MMR. The eccentricity posterior samples fall between the equilibria of simulations with $11 \lesssim K \lesssim 144$, indicated by the red arrows in Figure 5.

Finally, we also explicitly compute a corresponding K value for each sample in the posterior distribution, assuming it is in an equilibrium MMR configuration. For each posterior sample, we substitute the planet masses and eccentricities into Equation (8) and solve for the value of $K = \tau_\alpha/\tau_e$ that gives $\left. \frac{d}{dt} \mathcal{D} \right|_{\text{dis}} = 0$. While many posterior samples are not located exactly on the equilibrium line, the deviation is small so we nevertheless assign them the K value of the associated MMR configuration. Computing the K values of all posterior samples in this manner, we obtain the distribution shown in Figure 6. The 99% credible interval of $12 \lesssim K \lesssim 117$ for the distribution of K values in Figure 6 is generally in agreement with the 3σ bounds estimated by comparing the posterior eccentricities to N -body simulations in Figure 5.

4. DISCUSSION AND CONCLUSIONS

In this paper, we reanalyzed the recently extended data set of RV measurements from the planetary system HD 45364 and fit an RV signal to observations using an N -body dynamical model. We also investigated how the inferred dynamical state of the system can be influenced by the choice of model priors and by the assumed level of measurement noise. Finally, we explored possible scenarios for the migration history of HD 45364’s planets assuming an MMR configuration of the system.

Our conclusions are summarized as follows:

1. We demonstrate that model priors have a large influence on the inferred MMR state of HD 45364 by comparing the results of an MCMC simulation that adopted a typical uninformative prior to one that adopted a prior more strongly weighted toward small libration amplitudes (i.e., resonant

configurations). Furthermore, failure to properly account for instrumental jitter can lead to biased inference of libration amplitudes in general. In the case of HD 45364 specifically, orbital configurations with small libration amplitudes become disfavoured relative to those with large libration amplitudes if instrumental jitter is not appropriately accounted for. More observations in the future will help conclusively determine whether the system is deep in the 3:2 MMR.

2. We find that the current orbital configuration of the HD 45364 system is consistent with past smooth orbital migration and eccentricity damping resulting in capture into MMR. Furthermore, we estimate the ratio of migration to eccentricity damping timescales, $K = \tau_\alpha/\tau_e$, during this process was in the range $11 \lesssim K \lesssim 144$.
3. The large masses and closely spaced orbits of the planets in HD 45364 produce strong planet-planet gravitational interactions, which we leverage in our N -body dynamical model to break the $m \sin I$ degeneracy present in most RV observations. This allows us to constrain the masses of the planets to within a factor of ~ 1.5 of their median values and the inclination of the system to $\sin I \gtrsim 0.6$.

We emphasize that, at present, the data do not conclusively constrain the HD 45364 planets to be locked in the 3:2 MMR. Nonetheless, dynamical models with priors strongly weighted toward low libration amplitude configurations, the expected outcome of resonant capture via smooth migration, produce a quality of fit to the existing data that is nearly indistinguishable from the quality of fit obtained while adopting conventional uninformative priors. In principle, the full mathematical machinery of Bayesian model comparison could be deployed to ascribe a likelihood that the system’s planets reside in resonance. However, any quantitative determination of this likelihood would require apportioning prior probabilities to competing models with different assumptions about the system’s formation history. Since the current state of planet formation theory is far too uncertain to yield robust predictions for such prior probabilities, we have forgone any such quantitative Bayesian model comparison calculations. Instead, we simply note that the RV data for HD 45364 are wholly consistent with theoretical expectations for resonant planetary systems formed through a process of smooth, disk-induced migration. We envisage future application of the methods developed in this paper to other candidate systems with planets in or near MMR, including RV-detected systems

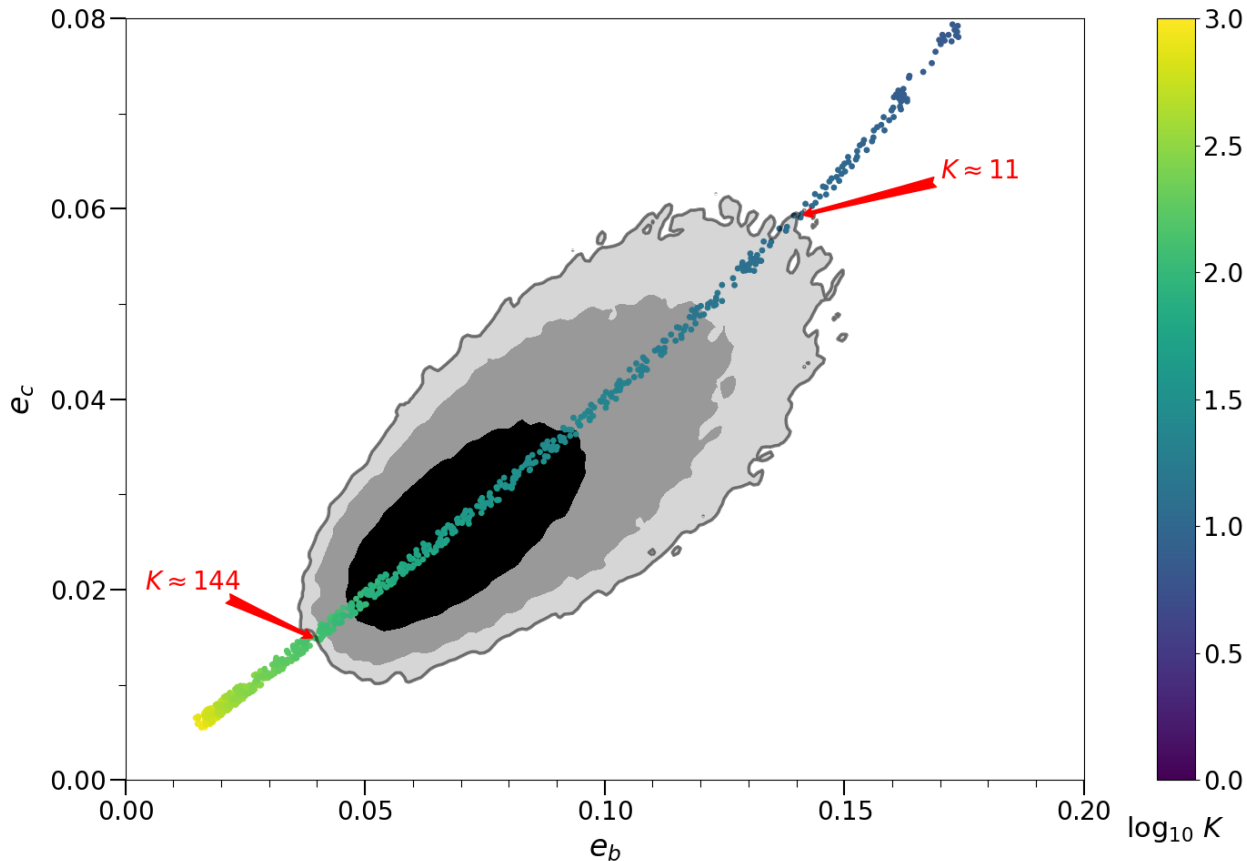


Figure 5. Comparison of our resonance capture simulations with the 2D marginalized distribution of planet eccentricities from the MCMC posterior of the resonance-weighted prior model described in Section 2.2 with $S = 0.1$. The 1σ , 2σ and 3σ contours of the posterior distribution are shaded. The simulated equilibrium eccentricity track using the best-fit planet masses is overlaid on the posterior distribution, with points falling within the MCMC posterior corresponding to simulated migration scenarios consistent with the observed eccentricities of the system. The approximate K values for the bounds of the overlapping track segment up to the 3σ contours are labeled as well, suggesting the orbital configuration of HD 45634 b and c could be reproduced with a value $11 \lesssim K \lesssim 144$.

(e.g. Wittenmyer et al. 2016; Luque et al. 2019; Rosenthal et al. 2019; Trifonov et al. 2019), transiting planet pairs (e.g. Dawson et al. 2021; Bozhilov et al. 2023) and higher-multiplicity resonant chains (e.g. Steffen et al. 2013; Mills et al. 2016; Luger et al. 2017; Leleu et al. 2021; MacDonald et al. 2021; Dai et al. 2023) in order to better understand the role of planetary migration in the formation history of these systems. In addition, we hope that our findings about the relationship between unmodeled RV measurement noise (instrumental jitter) and inferred libration amplitude will help inform studies of other resonant planetary systems.

5. ACKNOWLEDGMENTS

We thank Hanno Rein for helpful discussions. We thank Trifon Trifonov for a careful referee report that helped improve this manuscript. S.H. acknowledges support by the Natural Sciences and Engineering Research Council of Canada (NSERC), funding references CITA 490888-16 and RGPIN-2020-03885.

Software: REBOUND (Rein & Liu 2012), emcee (Foreman-Mackey et al. 2013), REBOUNDx (Tamayo et al. 2020)

REFERENCES

- Bozhilov, V., Antonova, D., Hobson, M. J., et al. 2023, The Astrophysical Journal Letters, 946, L36, doi: 10.3847/2041-8213/acbd4f
- Correa-Otto, J. A., Michtchenko, T. A., & Beaugé, C. 2013, Astronomy & Astrophysics, 560, A65, doi: 10.1051/0004-6361/201321917

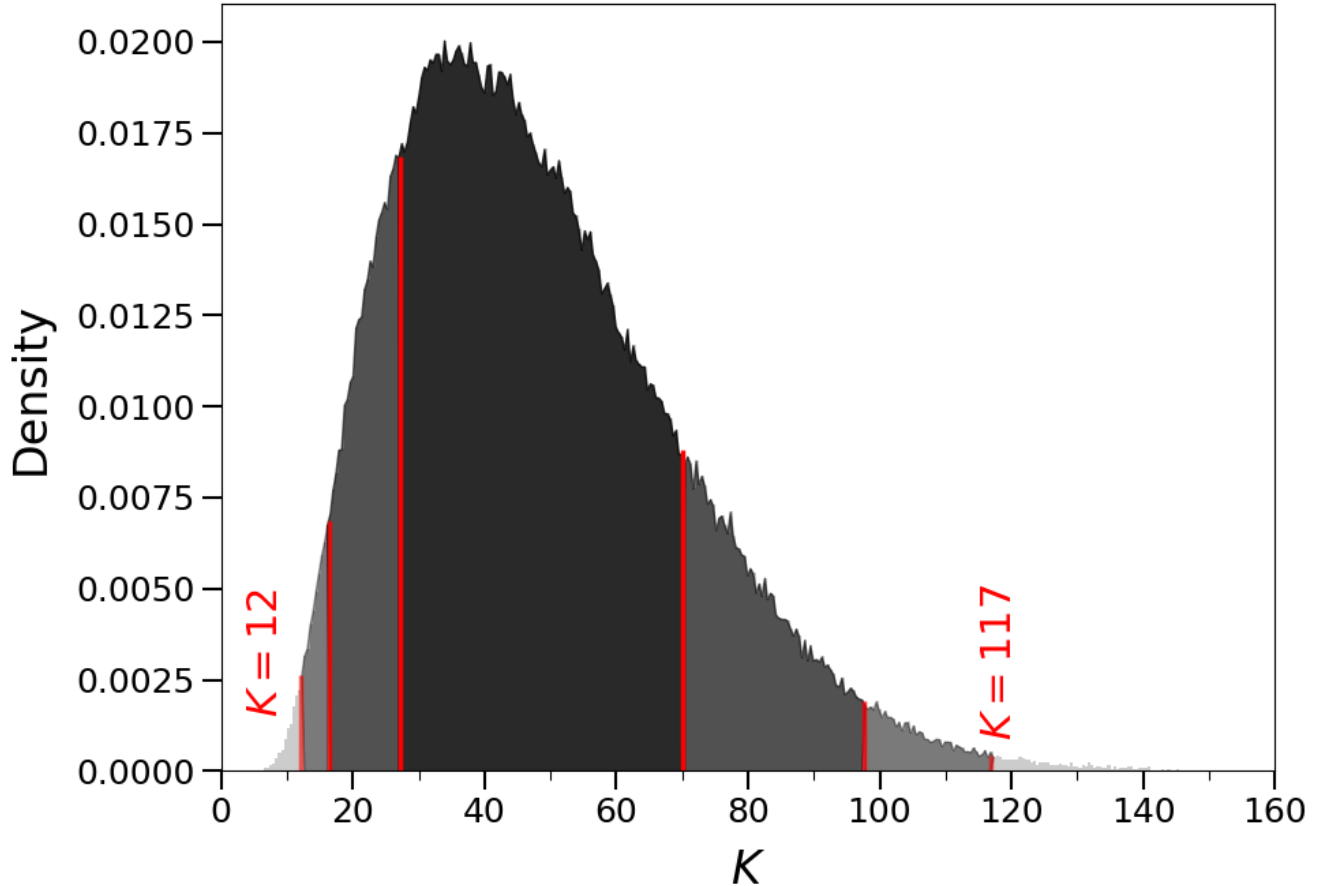


Figure 6. Density histogram of K values for the resonance-weighted prior model’s posterior eccentricity distribution shown in Figure 5, with the 68%, 95% and 99% credible intervals marked by red lines. The K values are computed from the posterior distribution using the method described in Section 3.2. The histogram yields $12 \lesssim K \lesssim 117$ as the 99% credible interval for the K values of possible migration scenarios, similar to the estimated bounds from the eccentricity track derived using N -body simulation in Figure 5.

- Correia, A. C. M., Udry, S., Mayor, M., et al. 2009, *Astronomy & Astrophysics*, 496, 521, doi: [10.1051/0004-6361:200810774](https://doi.org/10.1051/0004-6361:200810774)
- Dai, F., Masuda, K., Beard, C., et al. 2023, *The Astronomical Journal*, 165, 33, doi: [10.3847/1538-3881/aca327](https://doi.org/10.3847/1538-3881/aca327)
- Dawson, R. I., Huang, C. X., Brahm, R., et al. 2021, *The Astronomical Journal*, 161, 161, doi: [10.3847/1538-3881/abd8d0](https://doi.org/10.3847/1538-3881/abd8d0)
- Foreman-Mackey, D., Hogg, D. W., Lang, D., & Goodman, J. 2013, *Publications of the Astronomical Society of the Pacific*, 125, 306, doi: [10.1086/670067](https://doi.org/10.1086/670067)
- Giguere, M. J., Fischer, D. A., Payne, M. J., et al. 2015, *The Astrophysical Journal*, 799, 89, doi: [10.1088/0004-637X/799/1/89](https://doi.org/10.1088/0004-637X/799/1/89)
- Goldreich, P., & Tremaine, S. 1980, *The Astrophysical Journal*, 241, 425, doi: [10.1086/158356](https://doi.org/10.1086/158356)
- Goodman, J., & Weare, J. 2010, *Communications in Applied Mathematics and Computational Science*, 5, 65, doi: [10.2140/camcos.2010.5.65](https://doi.org/10.2140/camcos.2010.5.65)
- Hadden, S., & Payne, M. J. 2020, *The Astronomical Journal*, 160, 106, doi: [10.3847/1538-3881/aba751](https://doi.org/10.3847/1538-3881/aba751)
- Jensen, D., & Millholland, S. C. 2022, *The Astronomical Journal*, 164, 144, doi: [10.3847/1538-3881/ac86c5](https://doi.org/10.3847/1538-3881/ac86c5)
- Johnson, J. A., Payne, M., Howard, A. W., et al. 2010, *The Astronomical Journal*, 141, 16, doi: [10.1088/0004-6256/141/1/16](https://doi.org/10.1088/0004-6256/141/1/16)
- Johnson, J. A., Clanton, C., Howard, A. W., et al. 2011, *The Astrophysical Journal Supplement Series*, 197, 26, doi: [10.1088/0067-0049/197/2/26](https://doi.org/10.1088/0067-0049/197/2/26)
- Lee, M. H., Butler, R. P., Fischer, D. A., Marcy, G. W., & Vogt, S. S. 2006, *The Astrophysical Journal*, 641, 1178, doi: [10.1086/500566](https://doi.org/10.1086/500566)

- Lee, M. H., & Peale, S. J. 2002, *The Astrophysical Journal*, 567, 596, doi: [10.1086/338504](https://doi.org/10.1086/338504)
- Leleu, A., Alibert, Y., Hara, N. C., et al. 2021, *Astronomy & Astrophysics*, 649, A26, doi: [10.1051/0004-6361/202039767](https://doi.org/10.1051/0004-6361/202039767)
- Li, Z., Kane, S. R., Dalba, P. A., Howard, A. W., & Isaacson, H. T. 2022, *The Astronomical Journal*, 164, 163, doi: [10.3847/1538-3881/ac8d63](https://doi.org/10.3847/1538-3881/ac8d63)
- Lin, D. N. C., & Papaloizou, J. 1979, *Monthly Notices of the Royal Astronomical Society*, 186, 799, doi: [10.1093/mnras/186.4.799](https://doi.org/10.1093/mnras/186.4.799)
- Lo Curto, G., Pepe, F., Avila, G., et al. 2015, *The Messenger*, 162, 9, <http://www.eso.org/sci/publications/messenger/archive/no.162-dec15/messenger-no162-9-15.pdf>
- Luger, R., Sestovic, M., Kruse, E., et al. 2017, *Nature Astronomy*, 1, 1, doi: [10.1038/s41550-017-0129](https://doi.org/10.1038/s41550-017-0129)
- Luque, R., Trifonov, T., Reffert, S., et al. 2019, *Astronomy & Astrophysics*, 631, A136, doi: [10.1051/0004-6361/201936464](https://doi.org/10.1051/0004-6361/201936464)
- MacDonald, M. G., Shakespeare, C. J., & Ragozzine, D. 2021, *The Astronomical Journal*, 162, 114, doi: [10.3847/1538-3881/ac12d5](https://doi.org/10.3847/1538-3881/ac12d5)
- Mayor, M., Udry, S., Naef, D., et al. 2004, *Astronomy & Astrophysics*, 415, 391, doi: [10.1051/0004-6361:20034250](https://doi.org/10.1051/0004-6361:20034250)
- Mayor, M., Pepe, F., Queloz, D., et al. 2003, *The Messenger*, 114, 20, <http://www.eso.org/sci/publications/messenger/archive/no.114-dec03/messenger-no114-20-24.pdf>
- Mills, S. M., Fabrycky, D. C., Migaszewski, C., et al. 2016, *Nature*, 533, 509, doi: [10.1038/nature17445](https://doi.org/10.1038/nature17445)
- Murray, C. D., & Dermott, S. F. 2000, *Solar System Dynamics*, 1st edn. (Cambridge University Press), doi: [10.1017/CBO9781139174817](https://doi.org/10.1017/CBO9781139174817)
- Niedzielski, A., Nowak, G., Adamów, M., & Wolszczan, A. 2009, *The Astrophysical Journal*, 707, 768, doi: [10.1088/0004-637X/707/1/768](https://doi.org/10.1088/0004-637X/707/1/768)
- Petit, A. C., Petigura, E. A., Davies, M. B., & Johansen, A. 2020, *Monthly Notices of the Royal Astronomical Society*, 496, 3101, doi: [10.1093/mnras/staa1736](https://doi.org/10.1093/mnras/staa1736)
- Rein, H., & Liu, S.-F. 2012, *Astronomy & Astrophysics*, 537, A128, doi: [10.1051/0004-6361/201118085](https://doi.org/10.1051/0004-6361/201118085)
- Rein, H., Papaloizou, J. C. B., & Kley, W. 2010, *Astronomy and Astrophysics*, 510, A4, doi: [10.1051/0004-6361/200913208](https://doi.org/10.1051/0004-6361/200913208)
- Rein, H., & Spiegel, D. S. 2015, *Monthly Notices of the Royal Astronomical Society*, 446, 1424, doi: [10.1093/mnras/stu2164](https://doi.org/10.1093/mnras/stu2164)
- Robertson, P., Horner, J., Wittenmyer, R. A., et al. 2012, *The Astrophysical Journal*, 754, 50, doi: [10.1088/0004-637X/754/1/50](https://doi.org/10.1088/0004-637X/754/1/50)
- Rosenthal, M. M., Jacobson-Galan, W., Nelson, B., et al. 2019, *The Astronomical Journal*, 158, 136, doi: [10.3847/1538-3881/ab3b02](https://doi.org/10.3847/1538-3881/ab3b02)
- Snellgrove, M. D., Papaloizou, J. C. B., & Nelson, R. P. 2001, *Astronomy & Astrophysics*, 374, 1092, doi: [10.1051/0004-6361:20010779](https://doi.org/10.1051/0004-6361:20010779)
- Steffen, J. H., Fabrycky, D. C., Agol, E., et al. 2013, *Monthly Notices of the Royal Astronomical Society*, 428, 1077, doi: [10.1093/mnras/sts090](https://doi.org/10.1093/mnras/sts090)
- Tamayo, D., Rein, H., Shi, P., & Hernandez, D. M. 2020, *Monthly Notices of the Royal Astronomical Society*, 491, 2885, doi: [10.1093/mnras/stz2870](https://doi.org/10.1093/mnras/stz2870)
- Tinney, C. G., Butler, R. P., Marcy, G. W., et al. 2006, *The Astrophysical Journal*, 647, 594, doi: [10.1086/503706](https://doi.org/10.1086/503706)
- Trifonov, T., Tal-Or, L., Zechmeister, M., et al. 2020, *Astronomy & Astrophysics*, 636, A74, doi: [10.1051/0004-6361/201936686](https://doi.org/10.1051/0004-6361/201936686)
- Trifonov, T., Stock, S., Henning, T., et al. 2019, *The Astronomical Journal*, 157, 93, doi: [10.3847/1538-3881/aafa11](https://doi.org/10.3847/1538-3881/aafa11)
- Vogt, S. S., Allen, S. L., Bigelow, B. C., et al. 1994, in *Instrumentation in Astronomy VIII*, Vol. 2198 (SPIE), 362–375, doi: [10.1117/12.176725](https://doi.org/10.1117/12.176725)
- Wittenmyer, R. A., Tan, X., Lee, M. H., et al. 2013, *The Astrophysical Journal*, 780, 140, doi: [10.1088/0004-637X/780/2/140](https://doi.org/10.1088/0004-637X/780/2/140)
- Wittenmyer, R. A., Johnson, J. A., Butler, R. P., et al. 2016, *The Astrophysical Journal*, 818, 35, doi: [10.3847/0004-637X/818/1/35](https://doi.org/10.3847/0004-637X/818/1/35)
- Wright, J. T., Veras, D., Ford, E. B., et al. 2011, *The Astrophysical Journal*, 730, 93, doi: [10.1088/0004-637X/730/2/93](https://doi.org/10.1088/0004-637X/730/2/93)
- Zechmeister, M., Reiners, A., Amado, P. J., et al. 2018, *Astronomy & Astrophysics*, 609, A12, doi: [10.1051/0004-6361/201731483](https://doi.org/10.1051/0004-6361/201731483)